CHAPTER 183

Velocity measurements close to rippled beds

K.I. Mahesha Ranasoma ¹ and J.F.A. Sleath ²

Abstract

Velocity measurements have been made with a Laser Doppler Anemometer in oscillatory flow over rippled beds. The ripples were naturally formed in an oscillating tray rig and then stabilised.

Both large-scale mixing, repeatable from cycle to cycle, and turbulence were found to have a significant effect on the velocity profile. Large-scale mixing, which is associated with vortex formulation and ejection, was seen to dominate in the immediate vicinity of the bed but turbulent mixing appeared to be more important at large height. The variation in turbulence intensity with height was found to be qualitatively similar to that previously observed with threedimensional roughness in oscillatory flow. Time-mean velocities are not well predicted by existing theory. The present measurements show only two recirculating cells per ripple wavelength.

Introduction

The sea bed is frequently covered with ripples. Although much progress has been made in recent years there is still relatively little information about the way in which bed geometry changes the velocity distribution. It is the aim of the present investigation to provide more data. The results are relevant to problems such as sediment transport by waves, wave height attenuation and dispersion of pollutants in the sea.

Experimental apparatus and test conditions

The measurements were made in the apparatus described by Lee-Young and Sleath (1988). This consists of a steady flow flume with a section of bed which can oscillate with simple harmonic motion. In the present experiments

1 Graduate Student, Cambridge University Engineering Department, Trumpington Street, Cambridge CB2 1PZ, England. 2 Reader, ditto the steady flow was zero. The oscillating bed is 0.81m wide and 2.13m long. Disturbances generated by the ends of the bed are restricted by vertical baffles which effectively reduce the length of the working section to 1.17m. In the centre of the oscillating bed there is a sunken tray 0.70m wide x 0.70m long x 0.04m deep. Sand of medium diameter 0.41mm was placed in this tray. When the bed was oscillated at the chosen amplitude and period ripples formed on the sand. These ripples were stabilise by sprinkling with a thin coating of cement.

The velocity measurements were carried out with two different rippled beds. Bed 1 was formed by oscillating the tray with amplitude 78mm and period 2.45 secs. The ripples were of length, L, 100mm and crest-to-trough height, h, 18.4mm. Bed 2 was formed with amplitude of oscillation 40mm and period 1.25 secs. Ripple length was 50mm and height 9.1mm.

Fluid velocities were measured with a one-component DANTEC fibre-optic Laser Doppler Anemometer operated in backscatter mode. At each position the velocity was sampled 100 times per cycle for 50 cycles. Ensemble-average and root-mean-square velocities were then determined at each phase. At each position, horizontal velocity was measured first and then, by rotating the probe, the vertical velocity. Measurements were made at various vertical heights above the bed and at 11 horizontal positions (equally spaced over one wavelength of the ripple profile). The depth of water was 0.27m throughout.

Table 1 shows the test conditions. In this Table U_o is the amplitude of the velocity of the bed, T is the period of oscillation, a is the amplitude of oscillation, v is kinematic viconsity and b relates to the turbulence intensity (see below). Further details of the apparatus and test procedure are given by Ranasoma (1992).

Velocities

Fig 1 shows an example of the ensemble-average velocity vectors at various phases. The velocity of the bed is maximum at $wt=0^0$, 180^0 and zero at $wt=90^0$, 270^0 . The ripple profiles in this Figure and in Fig 8 are not to scale. They are shown only to indicate position relative to crest and trough.

Measurements were only made above the level of the crests. Even so, the vortex in the ripple lee is clearly shown in Fig 1(a). As the direction of the plate reverses (Fig 1(b)), we see that the lee vortex expands and then is carried back over the crest and into the trough beyond (Figs 1(c) and 1(d)).

As might be expected, the vortex dynamics have a significant effect on the velocity profiles. Fig 2 is an example of the horizontal defect velocity at various values of x and y and Fig 3 shows the corresponding curves for the vertical velocity. The broken lines in these Figures represent the theoretical velocity which would be found with this bed profile if the flow were inviscid. In Fig 3 we see that there is an upward surge in velocity, in comparison with the inviscid solution for $0 < w < 1 < 90^{\circ}$ at x / L = 0.4 (i.e just to one side of the crest). At the same time and position Fig 2 shows a decrease in horizontal velocity.

These changes are clearly association with the formation and ejection of a vortex on this side of the ripple crest. In comparison, the change in vertical velocity during the other half cycle (for $180^{\circ} < v < 270^{\circ}$) is insignificant because the vortex is then on the far side of the crest. Over the crest (x/L=0.5) and trough (x/L=0) the variations in vertical velocity are more or less the same in the two half cycles because these positions are affected equally by vortices formed on either side of the crest.

Large-scale mixing

Because of the clear influence of vortex formation and ejection on the velocity records it is to be expected that the large-scale exchanges in momentum associated with the vortices would have a dominant effect on the velocity profile. Since vortex formation and ejection repeats from cycle to cycle we will analyse this effect in terms of the ensemble-average components of velocity, u and v.

In order to facilitate comparison with the spatial-mean velocity, the spatialmean value of uv has been Fourier analysed. Fig 4 shows how the amplitude of the fundamental (i.e. the coefficient of $\cos \omega t$) varies with height. A mean line has been drawn through the experimental points in Fig 4. The equation of this line is

$$\frac{\dot{\Omega}}{U_0^2} = 0.09e$$
 -1.76ky -(1)

The origin for y is mid-height between crest and trough and $k=2\pi/L$.

There is also a variation in the phase of this fundamental component with height. If we draw a mean line through the experimental points for phase we obtain

$$\frac{1.76 \text{ky}}{\text{UV}} = 0.09 \text{e} \quad \cos(w \text{t-} 0.46 \text{ky-} 0.94) \quad -(2)$$

If momentum exchange due to large-scale mixing were the only important effect (in other words, if viscosity and turbulence were negligible) we would have

$$\frac{\partial U}{\partial t} = -\frac{\partial}{\partial y} (\overline{UV})$$
 -(3)

Where the overbar indicates the spatial-mean value (averaged in the horizontal direction). Making use of Eqns (2) and (3) we find that the variation with height of the spatial-mean velocity would be

Fig 5 shows how the amplitude of \overline{u} varies with height. Clearly Eq(4) significantly underestimates the measured values at large heights although the agreement is better as ky \rightarrow 0. The phase measurements in Fig 6 also show poor agreement with Eq(4).

We conclude that although large-scale mixing produced by the vortices may be the dominant effect at very small values of ky, other effects are more important further out. Since the flow was fully turbulent, viscous diffusion of momentum is negligible at large y. We must consequently examine turbulence.

Turbulence

Fig 7 shows how the root-mean-square components, u^{I} and v'_{i} of the horizontal and vertical fluctuations in velocity vary with height. These are the mean values, averaged in the horizontal direction and in time. Sleath (1991) found that for three-dimensional bed roughness the turbulent intensity in oscillatory flow was inversely proportional to height y_{1} , above the bed, in the same way as for grid-generated turbulence. In other words, with suitable choice of origin for y_{1} ,

$$\frac{1}{v'} = by_1 \tag{5}$$

Where b is a constant for any given test.

Fig 7 shows that reasonable straight lines can be drawn through the experimental points at vaues of ky greater than about 1 or 2. However, there is significant divergence from the straight line closer to the bed. The apparent origin for the straight lines is at ky=-0.58, which is the level of the troughs. Values of the coefficient b obtained from the slope of the experimental curves are shown in Table I.

The present tests do not cover a sufficient range of values of a, T and k_s , where k_s is the bed roughness length, for it to be possible to investigate whether b varies in the same way as for three-dimensional roughness. However, if we take k_s in the present tests equal to 4h the values of b in Table I are significantly smaller than corresponding values for three-dimensional bed roughness. This is hardly surprising in view of the difference in bed geometry.

In order to assess the effect of this turbulence on the velocity profiles we need to make some simplifying assumptions. Following Sleath (1991), we assume that the eddy viscosity is given by

$$\varepsilon_{\rm W} = {\rm v}'{\rm l}$$
 -(6)

where the mixing length I is given by

$$I = 0.1y_1$$
 -(7)

and y_1 has the same origin as in Eq(5). Substituting Eqns (5) and (7) into Eq (6) we see that ε_w does not vary with height. If momentum exchange due to turbulent mixing is the dominant effect we have

$$\frac{\partial \overline{u}}{\partial t} = \varepsilon_w \frac{\partial^2 \overline{u}}{\partial y^2} - (8)$$

consequently

$$\overline{u} = A e^{-\beta_1 y} \cos(\omega t - \beta_1 y - B)$$
 (9)

where A and B are constants and

 $\beta_1 = (\omega/2\varepsilon_w)^{1/2} = (5\omega b)^{1/2}$ -(10)

Making use of the values of b shown in Table I we obtain:

$$\beta_1/k = 1.37$$
 for tests 1,2,3,4
 $\beta_1/k = 1.86$ for tests 5,6,7
 $\beta_1/k = 1.11$ for test 8.

The corresponding curves obtained from Eq (9), assuming arbitrary values of the constants A and B, are shown in Figs 5 and 6. It is clear that the <u>slope</u> of the curves for amplitude and phase obtained from Eq (9) is in reasonable agreement with the measurements. Unfortunately we do not have any independent estimate for the values of A and B. Nevertheless, it seems reasonable to conclude that turbulence is the dominant effect on the spatial-mean velocity profile at large ky.

Time-mean velocity

So far we have been concerned with the oscillatory component of velocity. Fig 8 shows the time-mean Eulerian velocity vectors. As expected from the theoretical studies of Blondeaux and Vittori (1991) and others, we see recirculating fluid cells associated with each ripple wavelength. However, for the relatively large values of β L in the present experiments the theory predicts four cells per ripple wavelength instead of the two seen in Fig 8. Of course, there might be two cells below the lowest measured level. This is unlikely because these lower cells would be in the wrong direction for ripple formation and both inner and outer cells would be in directions opposite to those predicted by the theory. Equally, there might be re-circulating cells at larger values of y than shown in Fig 8 but the measurements of Sato et al (1984) and Horikawa and Ikeda (1990) show that this is not the case.

One possible reason for this discrepancy between theory and experiment is that the Reynolds numbers in the present tests are much larger than those for which theoretical mean streamlines have been calculated. Another possible reason is that, because of turbulence, the effective viscosity is much greater than the kinematic viscosity. Consequently, the effective value of β L is much smaller than the calculated value. For small β L the theory does indeed predict only one pair of re-circulating cells with directions of rotation similar to those in Fig 8.

The time-mean velocity is periodic in x. Fig 9 shows that the fundamental Fourier component (i.e. the term in cos kx) is dominant at all values of y for both the horizontal velocity \overline{u}_e and the vertical \overline{v}_e . The way in which the amplitude of this fundamental component varies with height is shown in Fig 10. Also shown in Fig 10 is the line corresponding to $\overline{v}_e \alpha \exp(-ky)$. The fact that the experimental points for a given test lie almost parallel to this line at large y is not surprising since L is the largest length scale and is consequently dominant far from the bed.

It will be seen from Table I that h/L is almost the same for all tests and, apart from Test 8, so is a/L. Consequently, the fact that the points do not lie along a single curve in Fig 10 is an indication that either Reynolds number or βL (or both) have a significant effect on the time-mean velocity.

Vorticity contours

Fig 11 shows vorticity contours calculated from the velocity measurements in Test $n^{\circ}2$. Fig 11(a) shows the lee vortex soon after maximum bed velocity. As the velocity reverses (Fig 11(b)) the vortex is forced out into the flow, carried over the crest (Fig 11(c)) and then on over the trough (Fig 11(d).

One interesting thing to emerge from these measurements is the relatively short life of the lee vortex once it has been pushed out from the bed by the reversing flow. In Fig 1(a), half way through the new half cycle, it is just possible to detect the old vortex to the right of the ripple crest but it is clear from Fig 11(a) that it is already very weak. This observation appears to contradict Bagnold's (1946) well-known photographs of vortex formation over rippled beds. In reality there is no contradiction. Bagnold's photographs show the trace left by the vortex in the aluminium powder on the water surface. Such a trace can remain long after the vortex which produced it has decayed to zero.

Conclusions

The velocity measurements close to rippled beds in oscillatory flow show the following results:

- (1) The flow patterns are strongly influenced by vortex formation and ejection. Nevertheless, the measurements show that the exchanges of momentum which are repeatable from cycle to cycle (i.e. not random) are not sufficiently large to explain the observed velocity profile, except in the immediate vicinity of the bed.
- (2) It is concluded that at large distances from the bed the flow is dominated by turbulence. For large y, turbulence intensity appears to be inversely proportional to height, in the same way as for three-dimensional bed roughness in oscillatory flow. A simple turbulence model shows reasonable agreement with the trend of the velocity measurements at large y.
- (3) Time-mean velocities are not well predicted by existing theory. The present measurements show only two re-circulating cells per ripple wavelength.
- (4) Patterns of vortex formation and ejection are similar to those described by other investigators. However, once the vortex has been ejected from the lee of the ripple into the flow above it appears to decay much more rapidly than is suggested by Bagnold's (1946) photographs.

References

Bagnold, R.A. (1946) 'Motion of waves in shallow water. Interaction between waves and sand bottoms'. Proc. Royal Society, London A187, pp1-18.

Blondeaux, P. and G. Vittori (1991): 'Vorticity dynamics in oscillatory flow over a rippled bed'. J. Fluid Mechanics, 226, pp257-289.

Horikawa.K and S.Ikeda (1990): 'Characteristics of oscillatory flow over ripple models'. Proc. 22nd Conf on Coastal Engng. ASCE, New York, pp661-674.

Lee-Young. J.S. and J.F.A. Sleath (1988): 'Initial motion in wave and current flows'. Proc.21st Conf on Coastal Engng. ASCE, New York, pp1140-1151.

Ranasoma. K.I.M. (1992): 'Measurements in combined oscillatory and steady flow over rippled beds'. Ph.d thesis. University of Cambridge. U.K.

Sato.S, Mimura.N. and A. Watanabe (1984): 'Oscillatory boundary layer flow over rippled beds'. Proc. 19th Conf. on Coastal Engng. ASCE, New York, pp2293-2309.

Sleath. J.F.A. (1991): 'Velocities and shear stresses in wave-current flows'. J.Geophys. Res. 96, NoC8, pp15237-15244.

Test	Ripple	h/L	а	Ť	U₀a	b	Symbol
	Length		mm	Sec	v	sec/m ²	
	<u></u>						
1	100	0.184	78	3.90	9320	935	0
2	100	0.184	78	2.41	14040	578	ā
3	100	0.184	78	1.70	19760	408	Δ
4	100	0.184	78	1.88	20480	451	
5	50	0.182	40	1.25	6680	2170	÷
6	50	0.182	40	2.47	3380	4290	×
7	50	0.182	40	1.80	4700	3130	*
8	50	0.182	80	2.45	14210	1520	
9	100	0.184	80	1.53	23900	358	e
10	100	0.184	80	2.00	18300	468	
11	100	0.184	80	3.02	12100	706	ē

Table 1. Test conditions

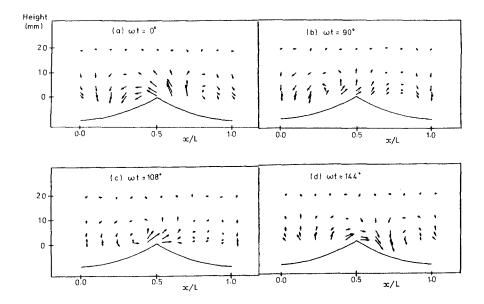
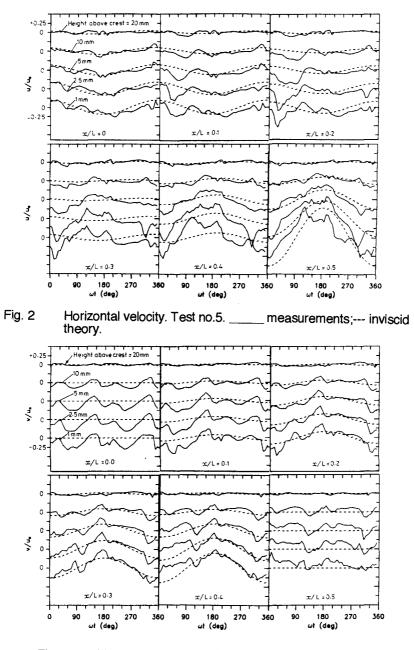


Fig. 1 Defect velocity vectors. Test no.5. (Ripple profile not to scale)





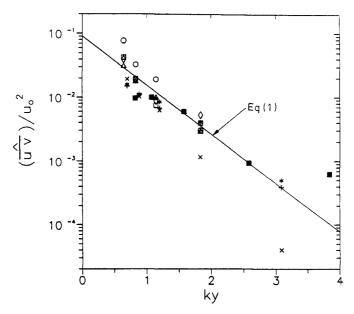


Fig. 4 Variation with height of the amplitude of the fundamental component of \vec{uv} . Symbols as in Table I

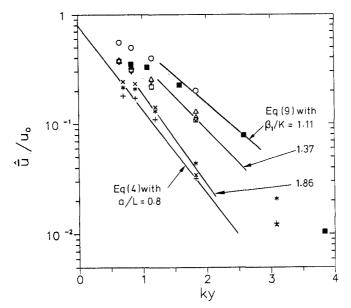


Fig. 5 Variation with height of the amplitude of the fundamental component of the spatial-mean velocity \overline{u} . Symbols as in Table I

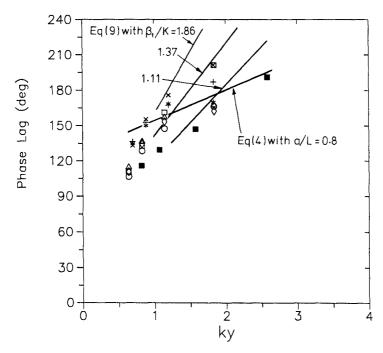


Fig. 6 Variation with height of the phase of the fundamental component of the spatial-mean velocity \vec{u} . Symbols as in Table I

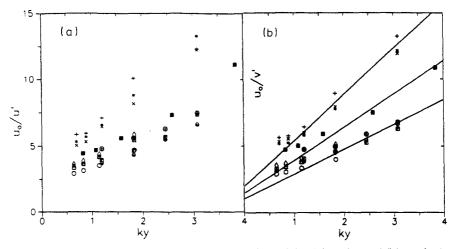


Fig. 7 Variation of turbulence intensity with height; (a) horizontal (b) vertical. Symbols as in Table I

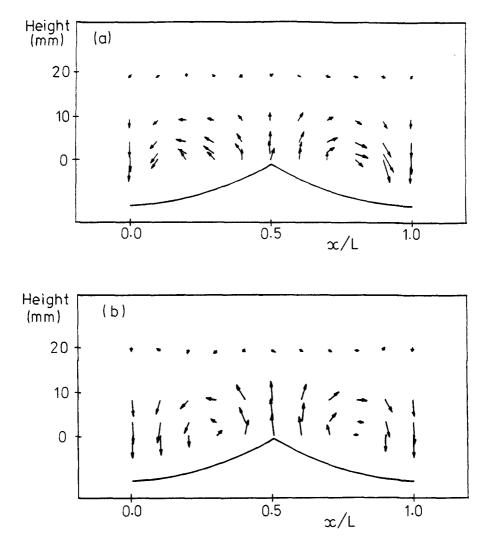


Fig. 8 Time-mean velocity vectors; (a) Test no.5 (b) Test no.2. (Ripple profiles not to scale).

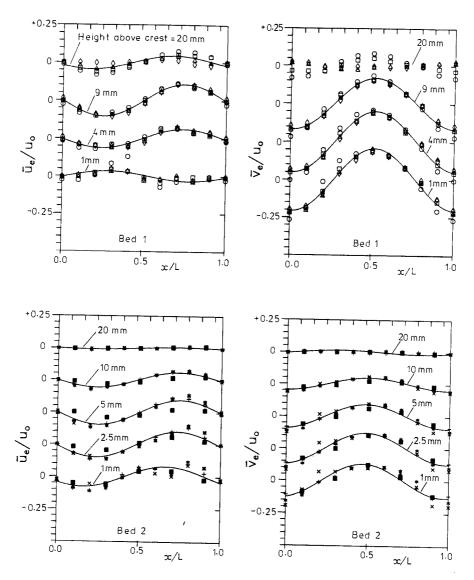


Fig.9 Spatial variation of the time-mean velocity. Symbols as in Table I

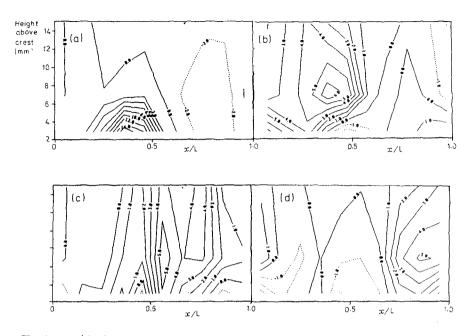


Fig.11 Vorticity contours for Test no.2; (a) $wt=7^{\circ}$ (b) $wt=94^{\circ}$ (c) $wt=140^{\circ}$ (d) $wt=157^{\circ}$

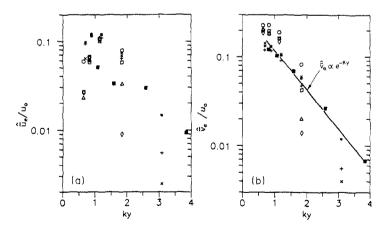


Fig.10 Variation with height of the amplitude of the fundamental component of the time-mean velocity; (a) horizontal velocity (b) vertical velocity. Symbols as in Table I